Noble-Metal Covered W(111) Single-Atom Electron Sources

I.-S. Hwang,[*,z] H.-S. Kuo, C.-C. Chang, and T. T. Tsong

Institute of Physics, Academia Sinica, Nankang, Taipei 115, Taiwan

Single-atom tips can be used as ideal point sources of electron beams. Noble-metal covered W(111) single-atom tips can be reliably prepared and their lifetimes are long enough for real applications. These tips are both thermally and chemically stable and can be regenerated in vacuum when accidentally damaged or contaminated. The atomic stacking remains the same each time it is regenerated. The small opening angle, smallest emitting area, high brightness, high spatial coherence, and high stability of these single-atom electron sources make them highly desirable for many applications. Both the brightness and spatial coherency of these electron sources are orders of magnitude better than those of the state-of-the-art electron sources used in electron microscopes. Application of these sources may significantly improve the performance and expand the capabilities of current electron microscopes and would probably open up many new possibilities in electron-beam based techniques.
© 2009 The Electrochemical Society.   [DOI: 10.1149/1.3269925] All rights reserved.

Electron-beam based instruments, such as scanning electron microscopes (SEMs) and transmission electron microscopes, are important in current technology. They allow observation and characterization of materials on a nanometer to micrometer scale. They even permit the fabrication of nanostructures and thus have been widely used in academia research as well as in industry. Improvement of their performance or development of instrumentation with capability has a great impact on the entire material sciences.

A major limitation on the performance of current electron-beam based techniques is the electron sources. Brightness and spatial coherence of electron sources are two key factors for their application to electron interferometry and holography,[1-4] electron diffraction,[5-7] and electron microscopies.[8] There have been demands for a higher brightness and a better coherency. Nanotips or single-atom tips (SATs) are of great interest for emitting coherent and bright electron beams because of their small source sizes. Use of these field emitters may greatly improve the resolution of the current electron microscopy. However, nanotips or SATs were very difficult to prepare. Several methods for producing SATs or nanotips were developed by different groups. However, those SATs or nanotips have never been put into practical applications because they suffer from short lifetimes and their preparation methods are tedious and very unreliable.

In this paper, the concept of nanotips and SATs and the traditional methods for preparation of nanotips are briefly reviewed, followed by our preparation method of a special type of SATs, noble-metal covered W(111) SATs, and determination of their atomic structures. These SATs are thermally and chemically stable and possess many desirable properties. Experiments for characterization of the spatial coherence of these single-atom electron sources are shown. We demonstrate total coherence (or full coherence), i.e., the transverse coherence width equal to or larger than the beam width, of these electron sources. Applications of these bright and highly coherent electron sources are discussed, which is then followed by the Conclusion.

Nanotips and SATs

Figure 1a illustrates electron field emission from a typical metal tip. It is a hemispherical tip with a radius r_{eff} of 50–100 nm. The half opening angle α is 35–50°. The brightness is defined as the current density per unit solid angle of the source.[8] That is, $\mathbf{B} = \mathbf{I}/[(\mathbf{dS})(\mathbf{d\Omega})] = \mathbf{I}/(\pi r_{eff}\alpha)^2$, where $\mathbf{I}$ is the field emission current, $\mathbf{dS}$ is the effective source size ($\mathbf{dS} = \pi r_{eff}^2$), and $\mathbf{d\Omega}$ is the solid angle subtended by the electron beam ($\mathbf{d\Omega} = \pi\alpha^2$). In general, a larger emission current, a smaller source size, or a smaller angular divergence would yield a higher brightness. A high brightness means a high current intensity when the beam is focused to a very small spot size.

In the 1960s, Gomer suggested that formation of a tiny protrusion on a hemispherical field emitter might produce a lens effect to confine the beam angular divergence.[9] Along with the smaller emitter source size, the beam brightness could be effectively increased. Many groups followed this concept and proposed various approaches to build up a nanoprotrusion on the tip apex, so called a nanotip. Enhancement of the beam brightness from nanotips has been confirmed. Figure 1b illustrates field emission from a nanotip. The half opening angle is much smaller than that of the typical hemispherical field emitter.

In general, a nanotip is a special type of electron field emitter and an SAT is a nanotip that ends with only one atom. It has been long considered that a smaller source size would yield a higher brightness and a larger transverse coherence width (also called spatial coherence length or lateral coherence width).[8,10,11] Therefore, nanotips can be very bright and highly coherent electron emitters. In principle, single-atom emitters would produce the brightest and most coherent electron beams. That is why much effort has been devoted to search nanotips or single-atom emitters.

In 1986, Fink prepared an SAT by field ion microscopy.[12,13] He first prepared a W(111) tip ended with only three atoms and deposited several tungsten atoms on the tip. He then field-evaporated excess atoms until only one atom remained at the top. In 1992, Binh and Garcia proposed a field-surface-melting method,[14] which involved repeated heating at a positive high electric field. Field ion microscopy is also used to monitor the atomic arrangement of the tip apex until a single atom stands on the top. Nagaoka et al. also fabricated a nanotip by applying a negative high electric field to a contaminated W⟨111⟩ tip.[15] There were also reports on the use of ion back bombardment[16,17] or a thermal field method[18-20] to obtain nanotips. All of these methods require tedious procedures and high technical skills. Moreover, a special instrument, such as a field ion microscope (FIM) or a field emission microscope (FEM), is required to monitor the tip condition in situ to stop the tip processing at the right time. The most serious problem is that these tips usually do not last long because their structures are neither thermally nor chemically stable. Thus, the application of nanotips or SATs is very limited so far.

Noble-Metal Covered W(111) SATs

Adsorbate-induced faceting.— In the 1990s, Madey and co-workers found that a flat W(111) substrate covered with an ultrathin Pd, Pt, Au, Ir, or Rh film can undergo massive reconstruction upon annealing to form three-sided pyramids with {211} facets.[21-24] The driving force of the facet formation was attributed to an increase in

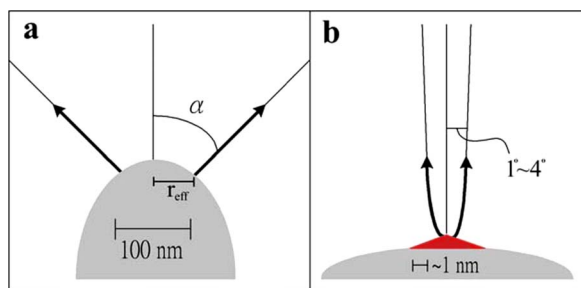* Electrochemical Society Active Member.
z E-mail: ishwang@phys.sinica.edu.tw

Figure 1. (Color online) (a) Field emission from a typical metal tip. (b) Field emission from a nanotip.

Figure 3. (Color online) Schematic diagram for preparation of a noble-metal covered W(111) SAT. (a) Etch a single-crystal W ⟨111⟩ wire to a tip shape. (b) Cover the tip with nail polish except for the apex. (c) Reduce native oxide by cathodic polarization. (d) Electroplate a noble-metal film on the tip under the condition of cathodic polarization. (e) Remove the nail polish and transfer the tip into the vacuum. (f) Anneal the tip to diffuse noble-metal atoms to other parts of the tip. (g) A pyramidal SAT builds up spontaneously.

surface energy anisotropy as the metal films were adsorbed on the W(111) surface, which was later confirmed by theoretical calculations.[25,26]

Pd-covered W(111) SAT.— Inspired by this adsorbate-induced faceting process, Fu et al. successfully prepared the first Pd-covered W(111) SAT by evaporating a Pd monolayer on a clean tungsten tip surface and then annealing the tip in ultrahigh vacuum (UHV).[27] Because the faceting is a thermodynamic process, the SAT can be regenerated by simple annealing even if it is destroyed or contaminated. This ensures a very long lifetime for the tip. The SAT is stable up to a temperature for its formation, i.e., ~1000 K. Most importantly, the stacking of the SAT remains the same after each regeneration. This indicates that the Pd/W(111) SAT has an atom-perfect and well-defined atomic structure, in contrast with previous SATs that never showed the same atomic stacking for the final several atomic layers.

The atomic stacking of the Pd-covered W(111) SAT was determined layer-by-layer with an FIM.[27] This SAT is basically a nanopyramid grown on top of a larger hemispherical tip. A model for the stacking of the topmost layers in the nanopyramid is shown in Fig. 2. The pyramid ends with a Pd atom on the top. The second layer consists of 3 Pd atoms, the third layer consists of 10 atoms with a center tungsten atom surrounded by 9 Pd atoms, and the fourth layer consists of 21 atoms with center 6 tungsten atoms surrounded by 15 Pd atoms. This structure can be viewed as a three-sided W(111) pyramid covered with a physical monolayer (PML) of Pd atoms.

Electrochemical method for deposition of a thin noble-metal film on a W(111) tip.— Although the Pd-covered W(111) SAT prepared by Fu et al. possesses many desirable properties, there are several requirements for its preparation. First, a clean (impurity and oxide
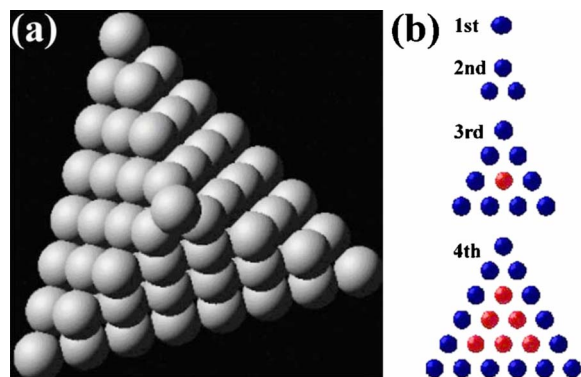
free) W(111) surface has to be prepared. Second, an appropriate amount of a noble metal (about 1 PML) has to be deposited on the clean tip surface. Third, the tip has to be annealed to an appropriate temperature to induce surface faceting. The third requirement can be carried out easily in most instruments that use field emission tips. However, the first two requirements are difficult to be fulfilled in most real applications, such as in electron microscopes, and make the application of this SAT less convenient.

A few years after the first preparation of the Pd-covered W(111) SAT, Kuo et al. presented another method with both the preparation of a clean W tip surface and the deposition of a noble-metal film in an electrochemical cell.[28-30] The procedure is illustrated in Fig. 3. This method can fulfill the above first two requirements outside the vacuum, which greatly simplify the preparation procedure.

Madey et al. pointed out that a proper coverage (~1 PML) of a noble-metal film on the W(111) surface is one of the prerequisites in inducing the faceting transition.[21-24] However, it is very difficult to control the coverage to exactly 1 PML due to the rather high deposition rate under cathodic polarization. This is because the electroplating has to be carried out at the potential for the native oxide reduction, which inevitably leads to a very high plating rate and a coverage much higher than 1 PML. To reduce the total amount of the plating material, the plated area is confined to a very small area around the tip apex with a nail polish. Typically, a noble-metal film of tens to hundreds of PMLs is deposited on a W(111) single-crystal tip apex.[28-30] As shown next, excess noble-metal atoms may diffuse to other parts of the tip surface which have not been plated during annealing in vacuum. Therefore, in this approach, the coverage of the noble-metal film is not as critical as what Madey et al. had found on flat W(111) surfaces.

FIM and FEM studies of noble-metal covered SATs prepared from electroplated W(111) tips.— The atomic structure at the tip apex can be imaged with an FIM, which has been described elsewhere.[31] Figure 4 shows FIM images of the atomic structure of a Pd-covered W(111) tip at different stages during processing in vacuum. After being degassed at 700 K for 5 min in our vacuum chamber, the as-deposited Pd-plated tip is imaged, as shown in Fig. 4a. Randomly scattered image spots indicate a rough tip surface. An ordered smooth tip surface gradually appears after annealing the tip to 1000 K for ~20 min (Fig. 4b). When the tip is annealed for another 5 min, the tip surface exhibits a ⟨111⟩ surface surrounded by other planes (Fig. 4c), which is a typical smooth tip surface seen on a body-centered cubic metal. This suggests that a Pd pseudomorphic overlayer is formed on the W tip.[30] An SAT shows up after further annealing to 1000 K for 5 min, as shown in Fig. 4d. The topmost atom can be field evaporated by increasing the positive voltage ap-

Figure 2. (Color online) Atomic model of the Pd-covered W(111) SAT determined by the field ion microscopy. (a) Top view of the pyramid with three {211} facets. (b) Atomic structure for the topmost four layers. Blue atoms are Pd and red atoms are W.
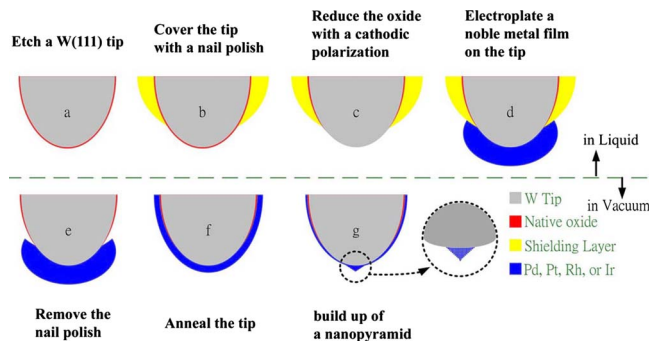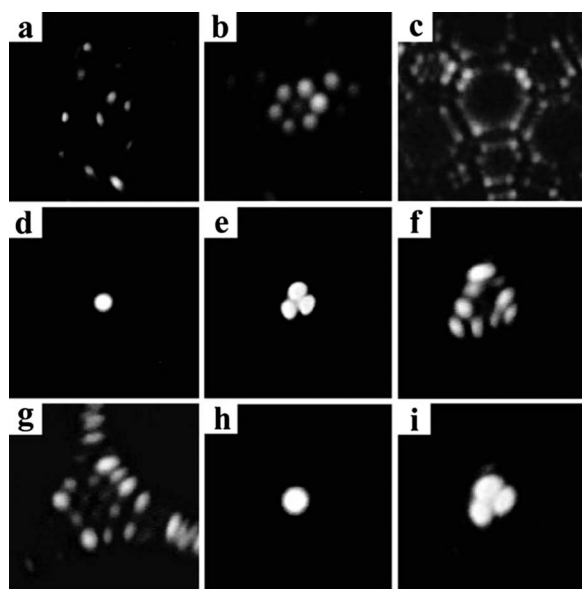
Figure 4. FIM images of a Pd-covered W(111) SAT prepared with the procedure outlined in Fig. 3. (a) As-deposited tip. (b) The tip after annealing at 1000 K for 20 min. (c) The tip after annealing at 1000 K for 25 min. (d) A Pd-covered W-(111) SAT is formed. (e) The second layer consists of three atoms. (f) The third layer consists of 10 atoms. (g) The fourth layer consists of 15 atoms. (h) A regenerated SAT by annealing to 1000 K for 5 min. (i) The second layer of the regenerated tip.

Figure 5. (Color online) FIM and FEM images showing the atomic structures of the tip apex and the corresponding electron field emission patterns, respectively. (a) FIM image of a Pd-covered SAT. (b) Field emission pattern of the Pd-covered SAT at −1100 V. (c) FIM image of a Pd-covered trimer tip. (d) Field emission pattern of the Pd-covered trimer tip at −1300 V. (e) FIM image of a Pt-covered SAT. (f) Field emission pattern of the Pt-covered SAT at −1300 V. (g) FIM image of a Pt-covered trimer tip. (h) Field emission pattern of the Pt-covered trimer tip at −1500 V. Scale bar indicates a length of 0.5 cm on the phosphor screen corresponding to 2° in the opening angle of the electron beam.

plied on the tip. Once the topmost atom is removed, the atomic structure of the second layer is exposed. We can apply an even higher voltage to remove the second layer and allow the third layer to be imaged. Therefore, the atomic structure can be imaged layer by layer with a series of field evaporations. Figure 4e and f shows 3 atoms on the second layer and 10 atoms on the third layer. Figure 4g shows only 15 atoms on the fourth layer, rather than 21 atoms as expected, because a few corner atoms are field evaporated together with the third layer of atoms. The FIM observations indicate that this is a pyramidal tip with three {211} facets. The atomic stacking of this SAT is the same as that reported by Fu et al. using vacuum deposition. The single-atom sharpness can be recovered simply by annealing the destroyed tip at 1000 K for 5 min. Figure 4h and i shows the regenerated pyramidal structure, which has an atomic stacking identical to the one before the field evaporation. This pyramidal SAT can be destroyed by the field evaporations and regenerated through annealing for several tens of times.

Pd-, Pt-, Ir-, Rh-, and Au-covered W(111) SATs were also successfully produced after the noble-metal plated tips were annealed in vacuum.[28-30] These pyramidal tips have the same structure as that of the Pd-covered W(111) SAT prepared by Fu et al.[27] and could be regenerated at least several tens of times after destruction by repeated field evaporations. Amazingly, the noble-metal plated tips can be stored in the ambient condition for more than 2 years before annealing in vacuum, which greatly simplifies the application of these SATs.

After checking the atomic structure of the tip with the FIM mode, we can switch to the FEM mode by pumping out the image gas and changing the polarity of the tip.[28] With the FEM mode, we can study the electron field emission pattern of a metal emitter. For a Pd-covered W(111) SAT, as shown in Fig. 5a, a circular spot subtending an angle of ∼6.6° [at full width at half-maximum (fwhm)] is seen with the FEM mode (Fig. 5b). The beam intensity profile, approximately Gaussian, is also superimposed on the emission pattern. This indicates that the electron emission originated from the topmost atom of the tip. When the topmost atom is removed by field evaporation, the second layer of a trimer is exposed
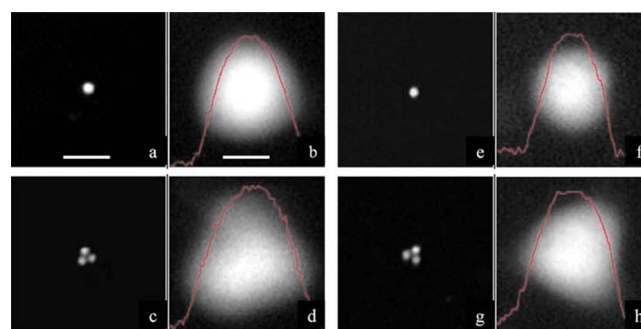
as in Fig. 5c. The corresponding electron field emission pattern also exhibits a triangular shape, as seen in Fig. 5d, indicating that the field emission mainly comes from the trimer.

For a Pt-covered W(111) SAT, the FIM and the corresponding FEM images are shown in Fig. 5e-h. The tip is very stable against the field emission, as in the case of Pd-covered W(111) tips. The field emission pattern measured on this Pt-covered W(111) SAT has an extension angle of ∼5.6°, slightly smaller than that of the Pd-covered W(111) SAT.

Brightness is proportional to the accelerating voltage. One can also define a reduced brightness $\mathbf{B_r} = \mathbf{B/V}$, which is a parameter independent of the accelerating voltage. From the above FEM measurements shown in Fig. 5, the reduced brightness for the Pd-covered W(111) SAT is estimated to be 2.2×10^8 A/m² sr V at the emission current of 1 nA.[28] The reduced brightness for the Pt-covered W(111) SAT is estimated to be 3.5×10^8 A/m² sr V at the emission current of 1 nA. If 100 keV is used as an accelerating voltage, the brightness of such emitters scales up to 2.2×10^{13} A/m² sr for the Pd-covered SAT and 3.5×10^{13} A/m² sr for the Pt-covered SAT, which are at least 1 order of magnitude higher than that of the W(111) buildup field emission gun at 100 keV (1.4×10^{12} A/m² sr).

Recent experiments by Ishikawa et al. showed that Pd-covered W(111) SATs could achieve a stable field emission as high as 20 nA.[32,33] The electron beams have very small opening angles of 2–3°, which make the brightness of these emitters (reduced brightness of 10^9–10^{11} A m⁻² sr⁻¹ V⁻¹) 1–4 orders of magnitude higher than that of the state-of-the-art electron sources, the Schottky emitter and the normal tungsten field emitter (reduced brightness of 10^7–10^8 A m⁻² sr⁻¹ V⁻¹).[8] It is also better than that of carbon nanotube emitters reported by de Jonge et al. (reduced brightness of ∼10^9 A/m² sr V).[34]

Chemical stability of noble-metal/W(111) pyramidal SATs.— The noble-metal plated W(111) tips can be stored under ambient conditions for at least 2 years before transferring them in vacuum for the preparation of SATs.[30] This is due to the protection of noble-metal thin films. To our surprise, noble-metal covered W(111) SATs are also chemically inert even though they are covered with only 1 PML of noble metals. These SATs can be exposed to the ambient conditions for more than 1 month. The SATs can be regenerated easily after mild annealing in vacuum. That means a noble-metal covered W(111) SAT prepared in a vacuum chamber can be brought to air and then transferred to another vacuum system.[30,33]
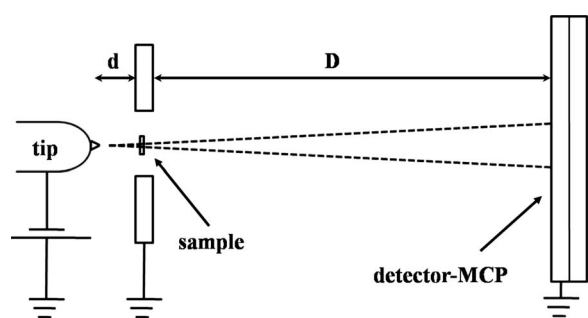
Figure 6. Schematic of the electron PPM. The electron beam is extracted from the topmost atom of the pyramidal SAT. The magnification of the sample at the screen is $(\mathbf{D} + \mathbf{d})/\mathbf{d}$, where $\mathbf{D}$ is 170 mm and $\mathbf{d}$ is the tip–sample separation.

Figure 7. (a) SEM image of a part of the microfabricated Si_3N_4 membrane. The width of hole is ~ 4.2 μm. (a) SEM image of a hole with suspended SWNTs.

Characterization of Noble-Metal Covered W(111) Single-Atom Electron Sources

The noble-metal covered W(111) SATs have been demonstrated to achieve a brightness significantly higher than the state-of-the-art electron sources used in current electron microscopes. Another important characteristic of electron sources is spatial coherence length or transverse coherence width. The high coherence and very high brightness of an electron source can significantly improve the performance of current electron microscopies. Especially, the phase coherence is crucial for electron interferometry, electron holography, and electron diffraction. Only when the electron beam is fully phase coherent, complete information contained in the phase can be retrieved. The coherence of an electron beam is mainly limited by the spatial coherence, not by the temporal coherence. The transverse coherence width ξ_T is typically estimated from the source size through the relation $\xi_T = \lambda D/\pi r_{eff}$, where λ is the electron wavelength and $\mathbf{D}$ is the distance between the source and the detector (or screen).[11,35] This relation suggests that a smaller source size would have a larger transverse coherence width. Experimentally, there are several methods to measure the spatial coherence of an electron source. A simple way we adopt here is to obtain the interference fringes of nano-objects with a low energy electron point projection microscope (PPM).[36,37] The contrast and the width of the interference fringes observed at high magnification reveal the spatial coherence of the electron source.

Low energy electron PPM.— Our experiments are carried out with a custom-made low energy electron PPM. The electron point projection microscopy is a shadow microscopy where an object is placed between a field emission electron point source and a screen. The shadow image of the object can be seen on the screen with a magnification equal to the ratio of the source–screen separation to the source–object separation. If the electron beam is coherent, interference fringes can be seen to be superposed on the shadow image.

Figure 6 shows a schematic of a custom-made electron PPM, which is housed in a UHV chamber made with mu metal. During our experiments, the sample holder is grounded and the tip is negatively biased to extract electrons from the tip end. The projected pattern is recorded with a multichannel plate (MCP, Hamamatsu F2226-24PGFX, 77 mm in diameter) and a phosphor screen, which are ~170 mm behind the sample. A charge-coupled device camera (Alta U2000, 1600 × 1200 pixels, 16 bit dynamic range) is used to take images on the screen.

Our sample holder is a microfabricated Si_3N_4 membrane coated with a Au film of 50 nm in thickness. Figure 7a shows an SEM image of a part of the membrane. The membrane contains periodic holes with a width of 4.2 μm, which allows suspension of single-walled carbon nanotubes (SWNTs) across the holes. Figure 7b shows an SEM image of a hole with suspended SWNTs. Only bundles of SWNTs can be seen in SEM images and isolated single SWNTs cannot be resolved.
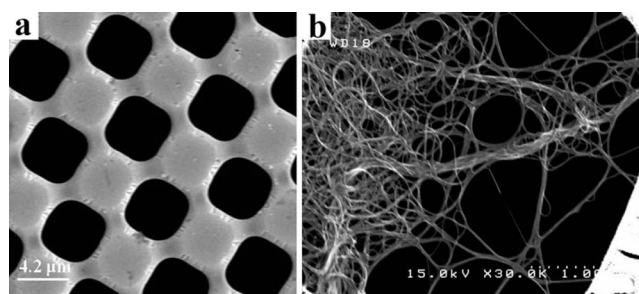
The tip used in our PPM experiments is an Ir-covered W(111) SAT. The tip holder is attached to a piezo-scanner that allows a fine movement in the X-Y-Z directions and the whole assembly is mounted on a stick–slip-type linear motor, as in scanning tunneling microscopy, to allow approaching of the tip to the sample.

Field emission pattern and PPM images from an iridium-covered W(111) SAT.— Figure 8a is a field emission pattern taken with an SAT at a voltage of −1400 V. The sample holder is removed in this case and thus the electron beam is extracted from the MCP 17 cm away. The pattern exhibits a round spot and the line profile of the intensity can be well fitted with a Gaussian distribution having standard deviation $\sigma = 4.5$ mm, as shown in Fig. 8c. The beam diameter
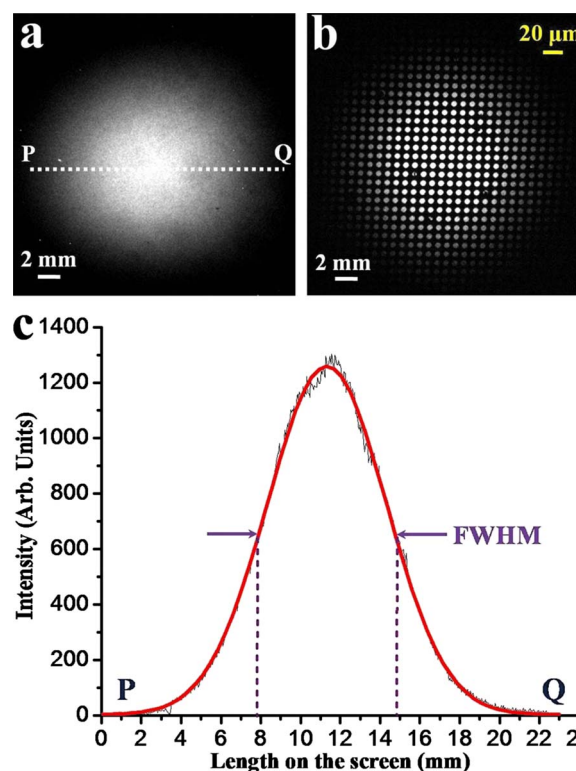

Figure 8. (Color online) Electron-beam profile of an Ir-covered W(111) single-atom emitter at room temperature. (a) Field emission pattern of the SAT at a tip voltage of −1400 V. The emission current is ~40 pA. The scale bar at the lower left corner indicates a length of 2 mm on the screen corresponding to an angle of 0.67°. (b) Point projection image of our sample holder when $\mathbf{d}$ = 4 mm. The tip bias is −500 V. The yellow scale bar at the upper right corner indicates a length of 20 μm on the sample plane. (c) Intensity profile of the field emission pattern along the dotted line PQ in (a) with fitting of a Gaussian distribution (the thick red curve).
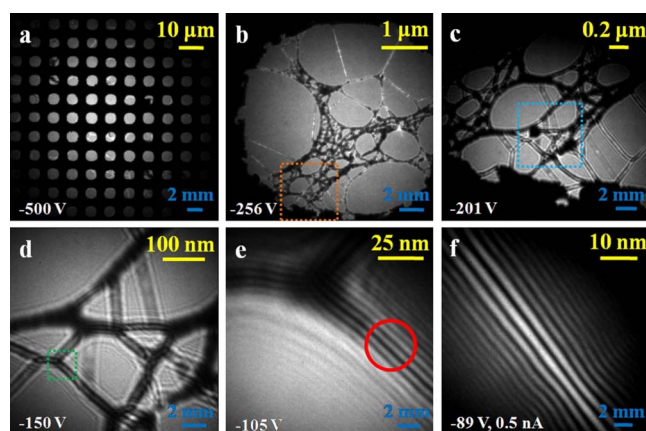
Figure 9. (Color online) Point projection images of interconnected SWNT bundles taken at different tip–sample separations. The tip and the sample are maintained at room temperature during imaging. (a) $d = 0.5$ mm. The tip bias is -500 V. (b) $d = 45$ μm. The tip bias is -256 V. (c) $d = 18.5$ μm. The tip bias is -201 V. (d) $d = 5$ μm. The tip bias is -150 V. (e) $d = 1.1$ μm. The tip bias is -105 V. (f) $d = 425$ nm. The tip bias is -89 V. The scale bar at the lower right corner indicates a length of 2 mm on the screen; the yellow scale bar at the upper right corner indicates a length as indicated on the sample plane.

is often defined as the fwhm, which is measured to be ~ 7 mm, corresponding to an opening angle (2α) of only 2.4°. Some people define the beam diameter as the full width at tenth maximum (FWTM). It is measured to be ~ 13 mm, corresponding to an opening angle (2α) of 4.3°. The fwhm value is similar to those obtained by Oshima et al. on several noble-metal covered W(111) SATs [32,33] and significantly smaller than those shown in Fig. 5. The larger measured opening angles in Fig. 5 may result from the narrow grounded bellow of the FIM system, which causes some broadening of the electron beams.

The projection image through the sample holder also exhibits a similar narrow beam profile, as seen in Fig. 8b when the tip is 4 mm away from the sample. The beam profile does not show any broadening compared with that in Fig. 8a even though the extraction distance is significantly smaller. The narrow beam profile remains almost the same even when the tip–sample spacing is less than 1 μm. This is another amazing point of this type of single-atom electron source.

When an Ir-covered W(111)SAT is moved closer to the sample, the projection image shows a higher magnification of the sample, which is inversely proportional to the tip–sample separation d. Figure 9a shows a projection image of the periodic holes of the sample holder taken at a tip voltage of -500 V. Some fine features related to SWNT bundles inside the holes can also be seen. By approaching

the tip to the sample, higher magnification images can be obtained. The tip voltage (or the extraction voltage) for field emission from the SAT also becomes smaller. The emission current is usually 10–50 pA when the extraction voltage is significantly greater than 100 V, but it increases to ~ 500 pA when the extraction voltage is about 100 V or lower due to the lower sensitivity of the MCP at low voltages. Figure 9b shows a higher magnification image of interconnected SWNT bundles inside a hole taken at a tip voltage of -256 V. Figure 9a-f clearly shows that the magnification increases with the decreasing tip–sample separation d. Also the tip voltage decreases with decreasing d. In Fig. 9c, interconnected SWNT bundles are seen. Notice that interference fringes around certain bundles can now be observed. The interference patterns of some bundles exhibit a strong contrast but there are also bundles exhibiting a weak contrast in their interference patterns. Figure 9d shows a PPM image taken at -150 V, corresponding to the region outlined with dashed lines in Fig. 9c. More interference fringes can be seen around these SWNT bundles. Figure 9f shows an image taken at a tip voltage of -89 V after a further approach toward the SWNT bundle indicated with a circle in Fig. 9e. Amazingly, the fringe pattern now spans throughout the entire bright area on the screen. More than 25 fringes are visible, as shown in Fig. 10a. An intensity profile XY across the fringe pattern is plotted in Fig. 10b. The oscillation in intensity can be seen throughout the entire beam with detectable intensity.

A common method to quantify the degree of coherence is the measurement of contrast from the interference fringes, where contrast $C = (I_{max} - I_{min})/(I_{max} + I_{min})$.[3,4,8] The better coherent the beam is, the larger C can be obtained. From the intensity profile in Fig. 10b, we obtain a value $C = 0.78$ with I_{max} taken as the maximum value of the highest peak and I_{min} as the minimum value of the valley next to it.[38] This value is higher than those (0.6–0.7) reported recently with a coherent source from a tungsten field emitter at 77 K [39] and far exceeds the values obtained with other sources. We note that the contrast value higher than 0.7 can be constantly obtained with this type of SATs. In the ideal case of interference from monochromatic plane waves with a uniform intensity in the lateral directions, C can reach a maximum value of 1. The reason our contrast is lower than 1 may come from several factors. One factor is the energy spread of our electron source, 0.3–0.4 eV,[33,40] which is slightly higher than that of a tungsten field emitter, 0.3 eV. Another factor may come from the contribution of inelastic scattering by the SWNT bundle of 10 nm in diameter, which is much larger than the inelastic mean free path (0.5–1.0 nm) for low energy electrons of ~ 100 eV.[41] Furthermore, the contrast value should be somewhat reduced for the very narrow Gaussian beam, in which the lateral intensity profile shows a strong decay away from the center.

The intensity profile shown in Fig. 10b suggests that the transverse coherence width could be equal to or larger than ~ 20 mm. This is significantly larger than the fwhm, FWTM, or 2σ measured in Fig. 8a. That means a good phase correlation across the entire
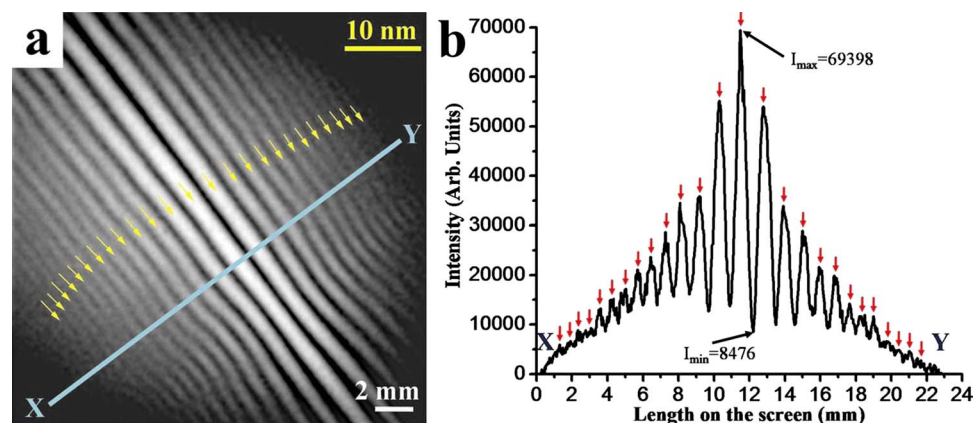

Figure 10. (Color online) (a) Processed PPM image shown in Fig. 9f. Each fringe is indicated with an arrow. Background signals, which are taken when the electron emission is turned off, have been subtracted pixel-by-pixel from the measured signals. (b) Intensity profile along the line XY.

beam width. Basically, the SWNT bundle can act as a nanoprism in a PPM.[39] The nanoprism splits the wavefront of an incoming electron wave into two coherent partial waves, which are deflected by the electric fields around the nanoprism in opposite directions and meet on the screen. Under normal action of a biprism, the fringes in the overlap region of the two waves are regularly spaced. The center three bright fringes in Fig. 10a exhibit the same spacing and very high contrast, suggesting that the central part of the beam is strongly phase correlated. The other fringes outside the center three may mainly result from the Fresnel edge interference, suggesting a good phase correlation between the center and the edge of the beam.

Traditionally, using the van Cittert–Zernike theorem, the coherence width can be estimated from the effective source size through the relation $\xi_T = \lambda D / \pi r_{\mathrm{eff}}$.[11,35] However, this theorem assumes that the effective source is a collection of mutually uncorrelated emission points. For an electron source with the beam divergence as in Fig. 8a and the electron energy of 89 eV, the smallest effective source size estimated from Heisenberg's uncertainty principle is ~ 3.9 Å, which is significantly larger than the real size of an SAT (1–2 Å).[38] Therefore, the electron beam emitted from the SAT can be considered as a beam from a perfect point source and thus should be fully (spatially) coherent. It is not physically meaningful to have any electron emission point smaller than this size. The estimation of the coherence width using the van Cittert–Zernike theorem is thus not appropriate when the real source size is equivalent to or smaller than the smallest size set by Heisenberg's uncertainty principle.

Applications of single-atom electron sources.— Both the brightness and spatial coherency of noble-metal covered W(111) single-atom sources are orders of magnitude better than those of the state-of-the-art electron sources used in current electron microscopes. Utilization of these fully coherent single-atom sources would significantly improve the performance of electron holography and coherent electron diffraction. This would have great impact on materials science and technology. In electron holography, the phase images allow quantitative determination of electric and magnetic fields in a material down to atomic dimension.[3,4] In coherent electron diffraction, methods have been developed to determine the three-dimensional atomic-resolution image of nonperiodic nanostructures.[5-7] In general, the more coherent the beam is, the better the quality of the high resolution phase contrast images, the sharper the diffraction patterns, and the better the diffraction contrast.

The very small opening angles of noble-metal covered W(111) single-atom sources provide additional benefits. It allows the operation of electron microscopes with good brightness even at low voltages because of very small spherical aberration. Low brightness at low voltages is a major limitation of current electron microscopes. Operation at a lower voltage would have higher image contrast for light elements, such as carbon, oxygen, and nitrogen, which are major elements in biological specimens. Development of low voltage electron microscopes would broaden the applications of electron microscopies. In addition, many electron-beam based instrumentations may be developed based on this type of high performance electron sources

Conclusion

The noble-metal covered W(111) SATs are promising candidates of electron sources in the future high performance electron-beam instruments. The total coherence and very high brightness of this type of single-atom sources can significantly improve the performance and expand the capabilities of current electron microscopies, electron interferometry and holography, and electron diffraction. We

anticipate that the fully coherent electron beam will also make possible many advanced electron-beam based experiments that are simply out of reach with current technology.

References

1. D. Gabor, *Nature (London)*, **161**, 777 (1948).
2. G. F. Missiroli, G. Pozzi, and U. Valdrè, *J. Phys. E: Sci. Instrum.*, **14**, 649 (1981).
3. A. Tonomura, *Rev. Mod. Phys.*, **59**, 639 (1987).
4. H. Lichte and M. Lehmann, *Rep. Prog. Phys.*, **71**, 016102 (2008).
5. J. Miao, T. Ohsuna, K. O. Hodgson, and A. O'Keefe, *Phys. Rev. Lett.*, **89**, 155502 (2002).
6. J. M. Zuo, I. Vartanyants, M. Gao, R. Zhang, and L. A. Nagahara, *Science*, **300**, 1419 (2003).
7. J. M. Zuo, M. Gao, J. Tao, B. Q. Li, R. Twesten, and I. Petrov, *Microsc. Res. Tech.*, **64**, 347 (2004).
8. D. B. Williams and C. B. Carter, *Transmission Electron Microscopy*, Plenum, New York (1996).
9. R. Gomer, *Field Emission and Field Ionization*, pp. 34–36, Harvard University Press, Cambridge, MA (1961).
10. N. García and H. Rohrer, *J. Phys.: Condens. Matter*, **1**, 3737 (1989).
11. M. R. Scheinfein, W. Qian, and J. C. H. Spence, *J. Appl. Phys.*, **73**, 2057 (1993).
12. H. W. Fink, *IBM J. Res. Dev.*, **30**, 460 (1986).
13. H. W. Fink, *Phys. Scr.*, **38**, 260 (1988).
14. V. T. Binh and N. Garcia, *Ultramicroscopy*, **42–44**, 80 (1992).
15. K. Nagaoka, H. Fujii, K. Matsuda, M. Komaki, Y. Murata, C. Oshima, and T. Sakura, *Appl. Surf. Sci.*, **182**, 12 (2001).
16. A. P. Janssen and J. P. Jones, *J. Phys. D*, **4**, 118 (1971).
17. R. Börret, K. Böhringerand, and S. Kalbitzer, *J. Phys. D*, **23**, 1271 (1990).
18. P. C. Bettler and F. M. Charbonnier, *Phys. Rev.*, **119**, 85 (1960).
19. V. T. Binh, *J. Microsc.*, **152**, 355 (1988).
20. K. Edinger, V. Yun, J. Melngailis, J. Orloff, and G. Magera, *J. Vac. Sci. Technol. B*, **15**, 2365 (1997).
21. K. J. Song, R. A. Demmin, C. Dong, E. Garfunkel, and T. E. Madey, *Surf. Sci. Lett.*, **227**, L79 (1990).
22. K. J. Song, C. Z. Dong, and T. E. Madey, *Langmuir*, **7**, 3019 (1991).
23. T. E. Madey, J. Guan, C. H. Nien, C. Z. Dong, H. S. Tao, and R. A. Campbell, *Surf. Rev. Lett.*, **3**, 1315 (1996).
24. T. E. Madey, C. H. Nien, K. Pelhos, J. J. Kolodziej, I. M. Abdelrehim, and H. S. Tao, *Surf. Sci.*, **438**, 191 (1999).
25. S. P. Chen, *Surf. Sci. Lett.*, **274**, L619 (1992).
26. J. G. Che, C. T. Chan, C. H. Kuo, and T. C. Leung, *Phys. Rev. Lett.*, **79**, 4230 (1997).
27. T. Y. Fu, L. C. Cheng, C. H. Nien, and T. T. Tsong, *Phys. Rev. B*, **64**, 113401 (2001).
28. H.-S. Kuo, I.-S. Hwang, T.-Y. Fu, J.-Y. Wu, C.-C. Chang, and T. T. Tsong, *Nano Lett.*, **4**, 2379 (2004).
29. H.-S. Kuo, I.-S. Hwang, T.-Y. Fu, Y.-C. Lin, C.-C. Chang, and T. T. Tsong, *e-J. Surf. Sci. Nanotechnol.*, **4**, 233 (2006).
30. H.-S. Kuo, I.-S. Hwang, T.-Y. Fu, Y.-C. Lin, C.-C. Chang, and T. T. Tsong, *Jpn. J. Appl. Phys., Part 1*, **45**, 8972 (2006).
31. T. T. Tsong, *Atom-Probe Field Ion Microscopy*, Chap. 3, Cambridge University Press, Cambridge (1990).
32. T. Ishikawa, T. Urata, B. Cho, E. Rokuta, C. Oshima, Y. Terui, H. Saito, A. Yonezawa, and T. T. Tsong, *Appl. Phys. Lett.*, **90**, 143120 (2007).
33. C. Oshima, E. Rokuta, T. Itagaki, T. Ishikawa, B. Cho, H.-S. Kuo, I.-S. Hwang, and T. T. Tsong, *e-J. Surf. Sci. Nanotechnol.*, **3**, 412 (2005).
34. N. de Jonge, Y. Lamy, K. Schoots, and T. H. Oosterkamp, *Nature (London)*, **420**, 393 (2002).
35. G. Pozzi, *Optik*, **77**, 69 (1987).
36. H. W. Fink, W. Stocker, and H. Schmid, *Phys. Rev. Lett.*, **65**, 1204 (1990).
37. V. T. Binh, V. Semet, and N. Garcia, *Appl. Phys. Lett.*, **65**, 2493 (1994).
38. C.-C. Chang, H.-S. Kuo, I.-S. Hwang, and T. T. Tsong, *Nanotechnology*, **20**, 115401 (2009).
39. B. Cho, T. Ichimura, R. Shimizu, and C. Oshima, *Phys. Rev. Lett.*, **92**, 246103 (2004).
40. E. Rokuta, H.-S. Kuo, T. Itagaki, K. Nomura, T. Ishikawa, B.-L. Cho, I.-S. Hwang, T. T. Tsong, and C. Oshima, *Surf. Sci.*, **602**, 2508 (2008).
41. A. Zangwill, *Physics at Surfaces*, p. 21, Cambridge University Press, Cambridge (1988).